J. Plasma Phys. (2022), *vol*. 88, 905880204
Published by Cambridge University Press
doi:10.1017/S0022377822000162

A canonical view on particle acceleration by electromagnetic pulses

F. Russman [1],†, **S. Marini** [2,3],† **and F.B. Rizzato**[1],†

[1]Instituto de Física, Universidade Federal do Rio Grande do Sul, Caixa Postal 15051, 91501-970 Porto Alegre, RS, Brasil

[2]LSI, CEA/DRF/IRAMIS, CNRS, École Polytechnique, Institut Polytechnique de Paris, F-91120 Palaiseau, France

[3]LULI, Sorbonne Université, CEA, CNRS, École Polytechnique, Institut Polytechnique de Paris, F-75252 Paris, France

(Received 31 August 2021; revised 14 February 2022; accepted 15 February 2022)

In the present work we investigate the dynamics of electrons under the action of wave packets of high-frequency electromagnetic carrier waves. When the group velocities of the packets are subluminal, electrons can be efficiently accelerated. We show that the whole process can be described by an accurate ponderomotive canonical formalism that includes relevant extensions of the original ponderomotive approach applied to carriers moving at the speed of light. Single-particle simulations validate our analytical approach and show that extended canonical methods provide better agreement with numerics than previous investigations. In particular, we obtain a precise relationship between the wave amplitude and group velocity for optimum acceleration of initially stationary targets.

Key words: plasma waves, intense particle beams, plasma nonlinear phenomena

1. Introduction

Moving packets of high-frequency electromagnetic carrier waves have been proposed in the past as efficient structures for acceleration and deceleration of charged particles in cases of both luminal (Startsev & McKinstrie 1997) and subluminal pulses (Liu & Tripathi 2005; Sazegari, Mirzaie & Shokri 2006).

If dissipative effects such as radiation reaction (RR) (Landau & Lifschitz 1965) are ignored, there can be no net acceleration in the luminal case, unless particles are created inside the pulse. Externally created particles caught up by the pulse are simply overtaken with no net acceleration.

In the subluminal case, the interesting central idea is to use the compact high-intensity pulse as a moving wall impinging on a target charged particle. Here, we note that acceleration in the conservative case is possible because particles can actually outrun the wave pulse after the interaction in accelerating regimes, or outrun the wave pulse before the interaction in decelerating regimes. If the pulse amplitude and the relative velocity between pulse and particle are properly chosen, particles are kicked (or scattered) by the

† Email addresses for correspondence: russman@ufrgs.br, samuel.marini@polytechnique.edu, rizzato@if.ufrgs.br

pulse and either accelerated to high speeds, or decelerated to minimum velocities. On the other hand, if scattering conditions are not met and dissipative effects such as RR dissipation are ignored, particles are again engulfed by the pulse and ejected at its far end with no net acceleration, similarly to the luminal case.

In many cases slightly subluminal pulses require carrier phase velocities just above the speed of light c, as for instance in wave-guiding systems (Elmore & Heald 1985). This introduces two different time dependencies in the wave–particle dynamics: the one associated with the pulse motion, and the one associated with the carrier's high-frequency behaviour. The pulse width is in general much larger than the carrier's wavelength, so the pulse dynamics in those cases can be viewed as a slow modulation superimposed on the amplitude of the high-frequency carrier.

Average ponderomotive approximations (Shukla *et al.* 1986; Mendonça 2001; Sazegari *et al.* 2006; Mulser & Bauer 2010; Smorenburg *et al.* 2010; Burton *et al.* 2017; Peng *et al.* 2020; Terzani *et al.* 2021) furnish the appropriate tool to deal with these two-time-scale dynamics and have been used in the investigation of pulses formed either with linearly or circularly polarized transverse carriers. The classic ponderomotive approach, based on fast time averaging of the dynamical equations, enables us to identify how the relevant control parameters correlate with the various wave–particle dynamical regimes. In particular, the explicit relationship between pulse amplitude and speed can be found to locate the transition from the accelerating, or reflective, regime, where particles are actually kicked by the pulse, and the passing regime, where particles simply traverse the pulse, ending up with the very same speed they had prior to the interaction, as outlined above. We point out that, although the passing regime is neutral in terms of overall acceleration in conservative approximations, it can be turned into an effective dumping or accelerating tool when dissipative effects are incorporated into the formalism. Estimates of the time interval during which the particle remains under the influence of the pulse, so crucial for these purposes (Di Piazza 2008; Harvey, Heinzl & Marklund 2011; Vranic *et al.* 2014), can be obtained from an accurate ponderomotive approach.

The ponderomotive approach can be written in terms of a proper canonical formalism. In the electromagnetic case of high-frequency waves moving at the speed of light, the one-dimensional ponderomotive Hamiltonian is simply the original Hamiltonian with the momentum and the field-dependent terms both replaced with their fast time averages (Macchi 1992; Terzani *et al.* 2021), as we will re-examine later. In our present case, however, neither the group velocity nor the phase velocity coincide with c; the former is smaller (hence, subluminal) and the latter is greater. Therefore, one needs to extend the original formalism, an extension that will bring some new terms and observable effects into the corresponding ponderomotive Hamiltonian formalism.

In the following sections we first introduce the full model to be investigated and develop the steps leading to a new set of variables where the high-frequency terms are absent. With our ponderomotive formalism thus obtained we then make comparisons with previous results from the literature, pointing out where the conventional and the canonical ponderomotive formalisms agree and where they disagree. Our results on the accurate canonical formalism are supported by the exact integration of the equations of motion.

2. General formalism

We now start the investigation by introducing the physical model we plan to study and the appropriate Hamiltonian formalism.

In the model we consider the effective one-dimensional (1-D) dynamics of a single particle moving along the x axis under the action of transversely polarized electromagnetic

https://doi.org/10.1017/S0022377822000162 Published online by Cambridge University Press

(EM) waves with vector potentials given in the forms

$$\boldsymbol{A}_{\rm circ} = A_0 \exp\left(-\frac{(x-v_g t)^2}{\sigma^2}\right)(\hat{\boldsymbol{y}}\sin\theta + \hat{\boldsymbol{z}}\cos\theta), \tag{2.1}$$

and

$$\boldsymbol{A}_{\rm lin} = \sqrt{2}A_0 \exp\left(-\frac{(x-v_g t)^2}{\sigma^2}\right)\hat{\boldsymbol{y}}\sin\theta, \tag{2.2}$$

respectively for the cases of circular (circ) and linear (lin) polarization. Transverse conserved canonical momenta along the fields are taken to be zero and the 1-D fast phase is introduced as $\theta \equiv kx - \omega t$, with k denoting the wave vector of the carrier and ω its frequency. As for the 1-D modulational profile, σ is the width of the packet with $k\sigma \gg 1$, and v_g the group velocity; we ignore packet dispersion. To implement the idea of superluminal carriers, we also consider a dispersion relation of the type $\omega = \sqrt{c^2k^2 + \omega_0^2}$, where ω_0^2 incorporates the effects of the finite transverse dimensions of a wave guide, a possible diffractive geometry related to focused laser beams in vacuum (Esarey *et al.* 1995; Steinhauer & Kimura 2003; Ralph *et al.* 2009; Lemos *et al.* 2018; Fedorov & Tzortzakis 2020) or the effects of a plasma medium (Elmore & Heald 1985). We note that TE_{01} and TE_{10} EM modes in a wave guide with rectangular cross-section produce a null in the axial magnetic field right at the cross-sectional midpoint. A thin electron beam injected in this region would therefore experience the effects of an approximate transversal plane wave. In both cases the phase velocity $v_\phi = \omega/k$ is superluminal and the group velocity $\partial\omega/\partial k$ is subluminal with $v_g = c^2/v_\phi$. For future convenience when the time comes for comparison of the two cases of polarization, we introduce the $\sqrt{2}$ in expression (2.2) such that the fast time intensity averages in both situations are the same; $\overline{\boldsymbol{A}_{\rm circ}\cdot\boldsymbol{A}_{\rm circ}} = \overline{\boldsymbol{A}_{\rm lin}\cdot\boldsymbol{A}_{\rm lin}}$, with the bar denoting the fast time (or fast phase) average defined as $\bar{g} \equiv (2\pi)^{-1}\oint g(\theta)\,{\rm d}\theta$ for a generic function $g = g(\theta)$.

Given the fields and the assumed geometry, the exact relativistic Hamiltonians for the circular and linear cases respectively read

$$H_{\rm circ} = \sqrt{1 + p^2 + A_0^2 \exp\left(-\frac{2(x-v_g t)^2}{\sigma^2}\right)}, \tag{2.3}$$

and

$$H_{\rm lin} = \sqrt{1 + p^2 + A_0^2 \exp\left(-\frac{2(x-v_g t)^2}{\sigma^2}\right)(1-\cos 2\theta)}. \tag{2.4}$$

Variable p denotes the canonical momentum along the canonical conjugate x axis, and from now on we work with the dimensionless rescaled variables $kx \to x$, $k\sigma \to \sigma$, $kct \to t$, $p/mc \to p$, $H_{\rm circ,lin}/mc^2 \to H_{\rm circ,lin}$, $v_g/c \to v_g$ and $qA_0/mc^2 \to A_0$. The phase variable θ simply preserves its adimensional and periodic nature and is now written in terms of the new dimensionless variables as $\theta = x - v_\phi t$ with $v_\phi \equiv \omega/(kc)$ as the dimensionless phase velocity of the carrier.

As we examine expressions (2.3) and (2.4) we promptly realize that (2.3) is ready for use. It is an exact expression already free of the fast phase θ, so we have an exactly integrable Hamiltonian (time can be canonically absorbed into coordinate x) that coincides with its ponderomotive averaged form (Sazegari *et al.* 2006).

Expression (2.4), on the other hand, is not free of θ. One thus cannot remove the time dependence from the Hamiltonian with one single canonical transform, as in the case of

https://doi.org/10.1017/S0022377822000162 Published online by Cambridge University Press

circular polarization, unless $v_g = v_\phi = 1$ (Startsev & McKinstrie 1997), which is not the case of interest here, as commented before. One has therefore a non-integrable system in the case of linearly polarized wave pulses.

The first attempt towards an analytic solution then would be to ignore the fast phase term, in which case one would recover the traditional ponderomotive Hamiltonian – let us call it $\bar{H}_0$ – given in terms of a slowly varying momentum driven by the average squared potential

$$\bar{H}_0 = \sqrt{1 + \bar{p}^2 + \overline{A^2}}, \tag{2.5}$$

with

$$\overline{A^2} = A_0^2 \exp\left(-\frac{2(\bar{x} - v_g t)^2}{\sigma^2}\right). \tag{2.6}$$

Under this approximation, the Hamiltonians for both circular and linear polarization cases would coincide. Note that in expression (2.6) we replace the coordinate x with its average form $\bar{x}$, which is allowed by the smooth space–time dependence of the slowly modulated pulse profile.

We will, however, see that, although the attempt embodied by expression (2.5) works fine for linearly polarized carriers travelling at the speed of light (Macchi 1992), it yields incorrect results when the carrier becomes superluminal.

To summarize, we shall study the cases of circular and linear polarization separately, developing the theoretical model alongside the proper numerical work.

Let us then start with the case of circularly polarized waves as described by Hamiltonian (2.3).

3. Analysis of the wave–particle dynamics

3.1. *Circular polarization*

Given the Hamilton equations $\mathrm{d}p/\mathrm{d}t = -\partial H_{\mathrm{circ}}/\partial x$ and $\mathrm{d}H_{\mathrm{circ}}/\mathrm{d}t = \partial H_{\mathrm{circ}}/\partial t$, the 1-D Hamiltonian (2.3) generates one conserved quantity that can be written in the form

$$-v_g p + H_{\mathrm{circ}} \equiv K_{\mathrm{circ}}\ [\mathrm{const.}]. \tag{3.1}$$

One can evaluate the constant value of K_{circ} by examining the dynamics long before the interaction when the charged particle and the moving pulse are far from one another; it reads $K_{\mathrm{circ}} = -v_g p_0 + \sqrt{1 + p_0^2}$ with $p_0 = p(t = 0)$. Long after the interaction, when particles and pulse are again far from each other, K_{circ} takes a similar form $-v_g p_f + \sqrt{1 + p_f^2}$. Now the initial momentum is replaced with the final particle momentum $p_f = p(t = t_f)$, with t_f as an instant of time far beyond the one where the interaction took place.

Equating both forms of K_{circ} and adequately manipulating the resulting quadratic equation for p_f, two generic roots can be obtained

$$p_f = p_0, \tag{3.2}$$

$$p_f = \frac{2\gamma_0 v_g - (1 + v_g^2)p_0}{1 - v_g^2}. \tag{3.3}$$

As said, both results are generic and must be examined in each particular context of the interaction. Under this perspective, (3.2) applies either to situations where the wave and particle do not catch up with each other, or to those cases where particles go through the wave packet emerging with the very same kinetic energy.

https://doi.org/10.1017/S0022377822000162 Published online by Cambridge University Press

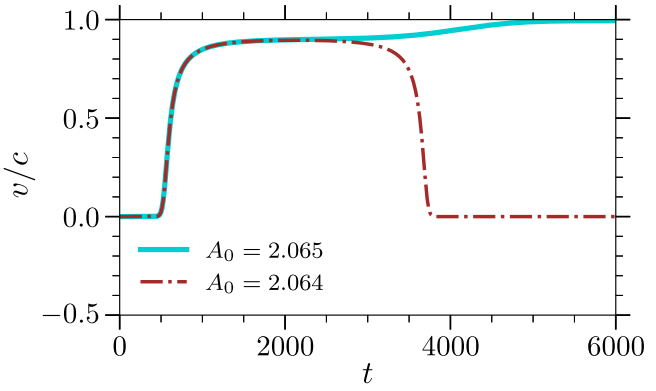

FIGURE 1. Velocity vs time. Two curves representing passing ($A_0 = 2.064$, dash-dotted brown curve) and reflected/accelerating ($A_0 = 2.065$, solid cyan curve) particles, for $v_g = 0.9$. The transition between the regimes is accurately expressed by the value obtained from (3.4).

On the other hand, (3.3) applies to cases where wave and particle catch up with each other and the wave amplitude is large enough to effectively scatter particles with subsequent changes in the latter's kinetic energy.

A useful test of the formalism is to find out the energy gain for an initially stationary particle as it is hit and accelerated by a packet of group velocity v_g and a given amplitude A_0. In this case, one needs the particle to be effectively scattered forward along the wave's moving direction. The critical condition guaranteeing that the particle will be continuously pushed forward, not going through the entire wave packet, is that $\dot{x} = v_g$ when the particle reaches the envelope peak at $x - v_g t = 0$ where the acceleration also vanishes: $\mathrm{d}p/\mathrm{d}t = -\partial H_{\mathrm{circ}}/\partial x = 0$.

This critical condition combined with the assumption of an initially stationary particle with $p_0 = 0$, imposes a minimum amplitude $A_{0,\mathrm{min}}$ for scattering, which is therefore tied to the group velocity in the form

$$A_{0,\mathrm{min}} = \frac{v_g}{\sqrt{1 - v_g^2}}. \tag{3.4}$$

Any amplitude larger than that will kick the particle into the forward direction, but smaller amplitudes will allow the particle to cross the entire packet, ending up with a null energy gain. The minimum amplitude can also be seen as a threshold between passing and reflective regimes for the particle dynamics, so we will occasionally refer to $A_{0,\mathrm{min}}$ as the threshold or critical amplitude as well.

We briefly illustrate the critical case just analysed with numerical integration of the equations of motion derived from the Hamiltonian (2.3), as presented in figure 1. There, we consider $\sigma = 100$ and $v_g = 0.9$, with $A_0 = 2.065$ for the solid cyan curve, $A_0 = 2.064$ for the dash-dotted brown curve and with initial conditions defined as $x_0 = 6\sigma$ and $p_0 = 0$. The choice $\sigma = 100$ satisfies the slow amplitude-modulation condition and is consistent with the value observed in the high-end laser pulses, (Papadopoulos *et al.* 2016). We will also show that the choice of different σ values implies qualitatively similar results, in the sense our theory still precisely describes the full 1-D particle simulations.

The critical amplitude is calculated from expression (3.4) as $A_{0\mathrm{min}} = 2.06474(\ldots)$, so the cyan (brown) curve represents the dynamics just above (below) the critical amplitude. We see that both curves behave as expected; particles are accelerated for the larger value of A_0, but end up with null speed for the smaller value.

https://doi.org/10.1017/S0022377822000162 Published online by Cambridge University Press

In addition, the final asymptotic velocity associated with the blue curve reads $v_{\text{numerical}} = 0.994475(\ldots)$, which coincides with the theoretical value predicted by expression (3.3), when adequately expressed in terms of the velocity given as $v_f \equiv v(t_f) = p_f/\sqrt{1+p_f^2}$.

One sees that, in the integrable case associated with circularly polarized EM pulses, the canonical formulation accurately describes the criticality features in a simple and straightforward way. We recall that, in this particular instance, the canonical approach coincides with that based on ponderomotive force arguments, as commented earlier.

As electrons are scattered, fully accelerated and pushed forward in the plasma, space-charge fields due to the ions left behind tend to pull the electrons back as a result of this snowplough effect (Robinson 2021). Although the accelerating regime must be reviewed in this case, the passing regime up to the transition point to acceleration may still be described by the pure ponderomotive theory. In a wave-guided environment, space-charge effects can be neglected.

Let us then proceed to the case of linear polarization where the canonical approach plays a crucial role, predicting observable deviations from the usual ponderomotive approach.

3.2. *Linear polarization*

As mentioned earlier, the full Hamiltonian (2.4) for the case of linear polarization contains an additional fast time dependence through the phase factor θ. This fast phase has space and time combined in a different way than in the slowly modulated amplitude. Under this circumstance, we are thus formally facing a non-integrable Hamiltonian system that cannot generate constants of motion along the lines discussed in § 3.1.

To obtain an integrable approximation of H_{lin} we use the canonical ponderomotive averaging approximation over the fast phase, which has been shown to describe the dynamics of the likewise averaged particle momentum and position in the centre-of-oscillation phase space (Mulser & Bauer 2010; Ruiz & Dodin 2017; Almansa *et al.* 2019). We recall that, since we are dealing with superluminal carrier waves, the final form of the averaged (or effective) Hamiltonian is expected to differ from the one arising in the case of carriers moving at the speed of light.

To proceed with the calculation, let us first consider the difference $H_{\text{lin}} - v_\phi p$, apply the full time derivative on it and take into account the appropriate canonical equations

$$\mathrm{d}H_{\text{lin}}/\mathrm{d}t - v_\phi\, \mathrm{d}p/\mathrm{d}t = \partial H_{\text{lin}}/\partial t + v_\phi \partial H_{\text{lin}}/\partial x. \tag{3.5}$$

Expression (3.5) contains fast and slow derivatives, the former coming from the fast phase and the latter coming from the slow amplitude modulations. By construction, the fast contribution cancels out, which leaves us only with the slow part. The quantity $H_{\text{lin}} - v_\phi p$ is therefore a slowly varying entity for which its fast phase average approximately coincides with its un-averaged value; if we call $H_{\text{lin}} - v_\phi p \equiv K_{slow}$ (slowly varying), one thus has, approximately, $\bar{K}_{\text{slow}} = K_{\text{slow}}$.

Now let us write $H_{\text{lin}} = v_\phi p + K_{\text{slow}}$, take its average and square the resulting expression. One has

$$\bar{H}_{\text{lin}}^2 = v_\phi^2 \bar{p}^2 + \bar{K}_{\text{slow}}^2 + 2 v_\phi \bar{K}_{\text{slow}} \bar{p}. \tag{3.6}$$

Let us then take the same expression $H_{\text{lin}} = v_\phi p + \bar{K}_{\text{slow}}$, first squaring it and then taking its average. Using the canonical form (2.4), one has

$$1 + \overline{p^2} + \overline{A^2} = v_\phi^2 \overline{p^2} + \bar{K}_{\text{slow}}^2 + v_\phi 2 \bar{K}_{\text{slow}} \bar{p}, \tag{3.7}$$

https://doi.org/10.1017/S0022377822000162 Published online by Cambridge University Press

which allows us to write expression (3.6) in the approximate form

$$\bar{H}_{\rm lin} = \sqrt{1 + \bar{p}^2 + \overline{A^2} + (1 - v_\phi^2)\,\overline{(\delta p)^2}}, \tag{3.8}$$

with $\overline{A^2}$ given by our early expression (2.6) and $\delta p \equiv p - \bar{p}$.

We now see that unless $v_\phi = 1$, the ponderomotive version of (2.4) can no longer be simply written as an effective Hamiltonian describing a particle of momentum $\bar{p}$ driven by the average squared EM potential as previously assumed in expression (2.5). A new fluctuational-type term $\overline{(\delta p)^2}$ (meaning the average of the squared fluctuation) is present and we need to unveil its role in the canonical dynamics.

The fluctuation δp arises from the action of the fast phase on the particle dynamics. One can estimate its time evolution from the canonical rules applied to $H_{\rm lin}$ in expression (2.4)

$$\dot{\delta p} = -(\partial H_{\rm lin}/\partial x)_{\rm fast} = -\partial H_{\rm lin}/\partial\theta. \tag{3.9}$$

If we approximate the phase factor as $\theta(t) = (\bar{v} - v_\phi)t$, where $\bar{v}$ is the slowly varying particle's velocity along x, one obtains

$$\delta p = \frac{A_0^2 \exp\left(-\dfrac{2(\bar{x} - v_g t)^2}{\sigma^2}\right)}{2\,(\bar{v} - v_\phi)\Gamma}\cos 2\theta, \tag{3.10}$$

and finally arrive at

$$\overline{\delta p^2} = \frac{A_0^4 \exp\left(-\dfrac{4(\bar{x} - v_g t)^2}{\sigma^2}\right)}{8\,(\bar{p}/\Gamma - v_\phi)^2\Gamma^2}, \tag{3.11}$$

where Γ and $\bar{v}$ are both calculated as their zeroth harmonic form $\Gamma = \sqrt{1 + \bar{p}^2 + A_0^2\,\mathrm{e}^{-2(\bar{x}-v_g t)^2/\sigma^2}}$, and $\bar{v} = \bar{p}/\Gamma$. Under these conditions an effective Hamiltonian depending only on slow variables can be obtained in the form

$$\bar{H}_{\rm lin} = \sqrt{\Gamma^2 - \frac{1}{8}\left(1 - \frac{1}{v_\phi^2}\right)\frac{A_0^4 \exp\left(-\dfrac{4(\bar{x} - v_g t)^2}{\sigma^2}\right)}{(\Gamma - \bar{p}/v_\phi)^2}}, \tag{3.12}$$

where the slowly varying variables $\bar{x}, \bar{p}$ are the new phase-space coordinates.

The effective Hamiltonian (3.12) was thus obtained from expression (3.8), with the new term $\overline{(\delta p)^2}$ calculated from (3.9), (3.10) and (3.11). The Hamiltonian can also be derived through a substantially more formal technique of canonical transformations (Goldstein 1980), much along the lines used in Ruiz & Dodin (2017) and Almansa *et al.* (2019), for instance. In this point of view, one seeks for a new canonical set of dynamical variables which are free from the θ-jitter induced by the high-frequency carrier. The corresponding calculations are described in appendix A and the final product of the appropriate canonical transformations is a Hamiltonian identical to (3.12).

To sum our results up to the present point, we have obtained an explicit form for the Hamiltonian $\bar{H}_{\rm lin}$ augmented by the new $\overline{(\delta p)^2}$ term. The final form for the Hamiltonian is given by expression (3.12), and the new term is the one preceded by the 1/8 factor in that expression. This term is absent both in the case of circular polarization and in the

https://doi.org/10.1017/S0022377822000162 Published online by Cambridge University Press

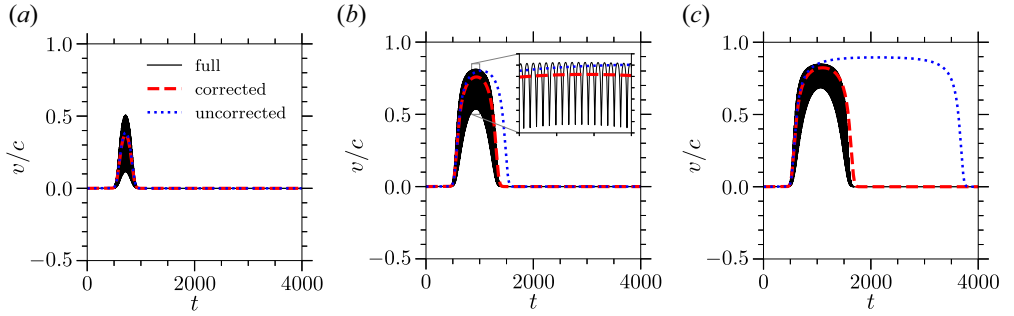

FIGURE 2. Evolution of the agreement between analytics and numerics represented by curves of velocity vs time for the initially stationary particle. We considered $v_g = 0.9$ in all cases, along with $A_0 = 1.0$ in panel (a), $A_0 = 1.9$ in panel (b) and $A_0 = 2.064$ in panel (c). Full simulations are depicted by the solid black line, the corrected model developed here by the dashed red line and the original uncorrected model by the dotted blue line. Even at larger values of A_0 neighbouring the transition from passing to reflected particles, the improved model keeps its nice agreement with simulations.

case of linearly polarized carriers moving with the speed of light, in which case $v_\phi = 1$. In the limit the phase velocity becomes luminal ($v_\phi = 1$), the driving wave no longer accelerate the electron, and both our model and the standard without correction fit well the 1-D particle simulations. Under this condition where the corrective term is absent, the ponderomotive Hamiltonian coincides with the form provided by Terzani *et al.* (2021) in their analysis focused on luminal waves with a large number of cycles within the pulse.

However, the new term is also omitted in cases where $v_\phi > 1$ as a lowest-order approximation, so we now set out to investigate its effects.

We first observe that, since we consider $v_\phi > 1$, the new term lowers the 'potential' associated with the sum of field dependent terms in Hamiltonian (3.12). Therefore, even though the new contribution to the potential function carries an additional complicated velocity dependence whose role cannot be predicted before integration, we expect to find higher field thresholds for the transition between the passing and reflective regimes discussed earlier. In particular, near the transition we expect the new term to affect the long stretches of time the particle spends under the influence of the pulse as it reaches for the unstable dynamical point at the peak of the potential. This will be information of particular relevance when RR effects due to acceleration (Smorenburg *et al.* 2010; Russman *et al.* 2020) are opportunely included in future works.

Let us then illustrate the role of the $\overline{(\delta p)^2}$ term in figure 2. Curves for velocity vs time obtained from full simulations (solid black line), the ponderomotive approximation with the $\overline{(\delta p)^2}$ corrective term (dashed red line) and the ponderomotive approximation without the corrective term (dotted blue line) are seen for three choices of field amplitudes A_0, all panels again with $v_g = 0.9$, $\sigma = 100$ and the same conditions of the previous case pictured in figure 1. Here, the full simulation case is given by the numerical integration of the equations from the Hamiltonian (2.4) while the cases with/without the correction term are given by the Hamiltonian (3.8), including/not including the term $\overline{(\delta p)^2}$ given by (3.11).

When fields are sufficiently low, as in the case $A_0 = 1.0$ of panel (a), all regimes are passing regimes, and both ponderomotive versions agree fairly well with the fully simulated curve. As the amplitude A_0 increases, one sees from panel (b) that, while the extended ponderomotive approximation still provides an accurate description for the

https://doi.org/10.1017/S0022377822000162 Published online by Cambridge University Press

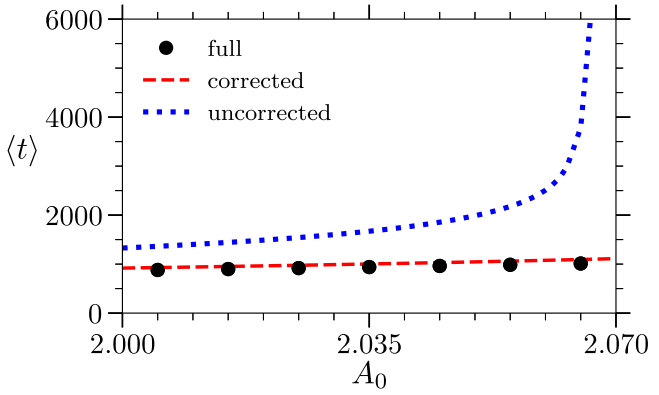

FIGURE 3. Transit times vs A_0 for simulations (black dots), the corrected ponderomotive model (dashed red line) and the uncorrected model (dotted blue line); $v_g = 0.9$. As already suggested from figure 2, the improved model maintains better agreement with particle simulations.

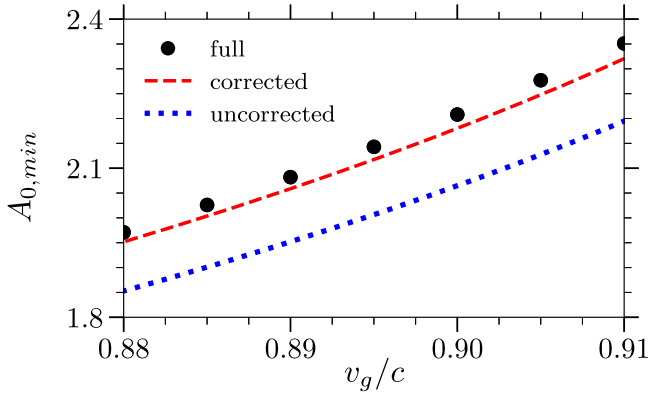

FIGURE 4. The amplitude threshold values as a function of v_g for the simulations (black dots), the corrected model (dashed red line) and the uncorrected model (dotted blue line). Once again the figure expresses the better accuracy of the improved theoretical calculations.

exact theory, the conventional approximation without the $\overline{(\delta p)^2}$ correction begins to reveal its limitations. If one keeps pushing A_0 up to larger values, as in panel (*c*), it is seen that the usual ponderomotive approximation reaches for the edge of the transition to reflective regimes much earlier (i.e. for noticeably smaller values of A_0) than the extended ponderomotive model. This is seen as the blue curve tends to remain for longer stretches of time nearest the peak of the potential, before crossing over and going back to the initial zero speed at the far side of the potential bump. However, even in these circumstances, the ponderomotive dynamics with the $\overline{(\delta p)^2}$ extension still agrees well with results of full simulations.

We thus see that the transit time the particle spends under the action of the pulse is highly dependent on the model as well as on the peak amplitude of the packet, both features related to the neighbouring presence of the unstable dynamical equilibrium at the envelope peak,

Given the relevance of the transit time, and with a basis on figure 2, we now try to quantify the amount of time the particles spend under the action of the wave pulses.

https://doi.org/10.1017/S0022377822000162 Published online by Cambridge University Press

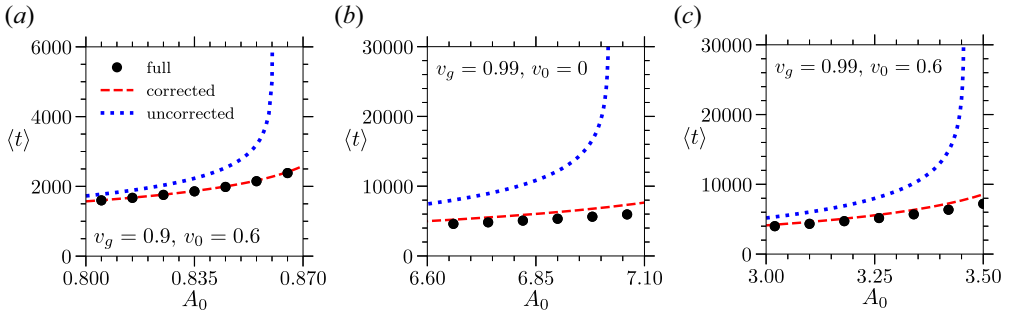

FIGURE 5. Transit times vs A_0 for simulations (black dots), the corrected ponderomotive model (dashed red line) and the uncorrected model (dotted blue line) assuming (*a*) $v_g = 0.9$, $v_0 = 0.6$, (*b*) $v_g = 0.99$, $v_0 = 0$, (*c*) $v_g = 0.99$, $v_0 = 0.6$ and $\sigma = 100$. The results suggest our model fits better the simulations independently of the wave phase velocity and the initial particle velocity.

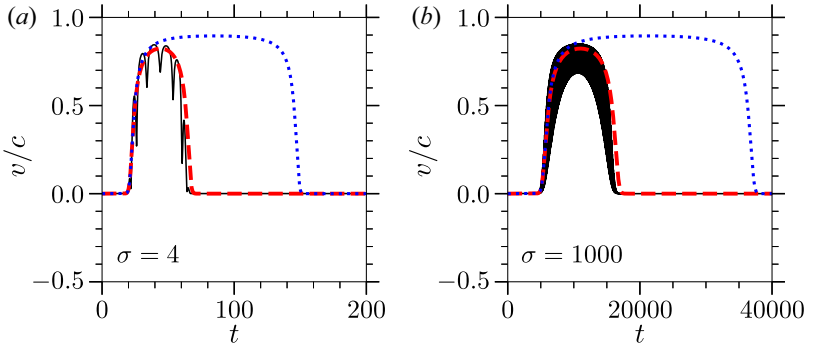

FIGURE 6. Evolution of the agreement between analytics and numerics represented by curves of velocity vs time for the initially stationary particle. We considered $v_g = 0.9$ and $A_0 = 2.064$ (see figure 2*c*) in all cases, along with $\sigma = 4$ in panel (*a*) and $\sigma = 1000$ in panel (*b*). Full simulations are depicted by the solid black line, the corrected model developed here by the dashed red line and the original uncorrected model by the dotted blue line. For different σ scales a nice agreement of our model with full simulations is observed.

The corresponding analysis is represented in figure 3, where curves are obtained from the proposed expression for the transit time $\langle t \rangle$

$$\langle t \rangle = \frac{2}{\sqrt{\pi}} \int_0^\infty \exp\left(-\frac{(x(t) - v_g t)^2}{\sigma^2} \right) \mathrm{d}t. \tag{3.13}$$

Expression (3.13) is a pulse profile weighted time counter. The infinity symbol here actually represents a sufficiently long time allowing particles to attain constant velocity after the interaction, and $x(t)$ is respectively obtained from full simulations, from the model without the $\overline{(\delta p)^2}$ correction and from the model with the $\overline{(\delta p)^2}$ correction. In the artificial case of a stationary particle with a constant $x \gg \sigma$, one would obtain the reasonable and expected value $\langle t \rangle = \sigma / v_g$; in the general case $\langle t \rangle$ is a measure of the time width of the plateaus or bumps of the previous figure 2.

Once again we see that the present extended model has better agreement with the full 1-D particle simulations.

https://doi.org/10.1017/S0022377822000162 Published online by Cambridge University Press

Given the sensitivity of the threshold amplitude (where $\langle t \rangle$ diverges to infinity) on the model, as seen in figures 2 and 3, we finally add a plot of the field threshold $A_{0,\min}$ vs v_g in figure 4. In the figure we depict the corresponding behaviours of both models and the simulations. The analytical full lines of the plot are obtained under the very same conditions used to derive expression (3.4): $v(x - v_g t = 0) = v_g$; and $\bar{H}_{\rm lin} - v_g \bar{p} = \text{const.}$, which is still true for our extended Hamiltonian depending only on the combination $x - v_g t$. The only difference now is that we solve the system numerically due to its involved algebraic structure resulting from the non-trivial form of Hamiltonian (3.12).

Again, the corrected model fits much more accurately the simulation points than its uncorrected counterpart.

We finally provide a brief discussion on the role of the initial velocity in the accelerating particle process. In figure 5, all cases are of accelerating particles and $\sigma = 100$. We see from figure 5(*a*) that the present theory keeps its accuracy, even at higher initial speeds (i.e. $v_0 = 0.6$, and $v_g = 0.9$). Interestingly, now increasing the group velocity would suggest that our correction should be of less significance due to the prefactor $1 - 1/v_\phi^2$. However, in such a scenario the wave amplitude needed to keep the reflective/accelerating regime must be higher, which ultimately implies that our corrections remain quite appreciable if, again, one remains in accelerating regimes. This is indicated in figures 5(*b*) and 5(*c*), where $v_g = 0.99$ and $\sigma = 100$, with $v_0 = 0$ in (*b*) and $v_0 = 0.6$ in (*c*). Moreover, the presented theory still holds even in the counter-directional scenario, where the electron moves towards the carrier (Vranic *et al.* 2014).

Finally, in figure 6 curves are displayed for velocity vs time obtained from full simulations (solid black line), from the ponderomotive approximation with the $\overline{(\delta p)^2}$ corrective term (dashed red line) and from the ponderomotive approximation without the corrective term (dotted blue line). A short laser pulse with $\sigma = 4$ is shown in panel (*a*), and a long pulse with $\sigma = 1000$ is shown in panel (*b*). The correction investigated in the present work indicates that our theoretical model, although formally constructed for high-frequency carriers, is in practice good for a wide range of the normalized envelope lengths σ.

4. Conclusions

In the present paper we studied the collisional dynamics of radiation pulses impinging on electrons, from a canonically oriented point of view. In addition to the appropriate full particle simulations, we developed an extended Hamiltonian ponderomotive treatment that takes into account the subluminal character of the pulse. The Hamiltonian developed here agrees with its original counterpart valid for pulses travelling at the speed of light, but, importantly, includes new relevant terms that become active for subluminal wave packets. With the inclusion of the new terms, the extended, or corrected, Hamiltonian provides significantly better agreement with full simulations.

The present model is purely conservative. However, since the analytical approach developed here describes much more accurately the time interval during which the particle remains under the action of the radiation packet, we expect to have a better understanding of RR dissipative effects, which depend on the extension of the wave packet and the corresponding time interval. As mentioned earlier, our model needs a thin beam injected at the centre of rectangular wave guides transporting the lowest-order modes. This is the way the beam sees a local planar wave with transverse polarization, for which case the theory applies. Otherwise, one would need to consider off-axis effects like transverse particle dynamics, and transverse dependence of the field amplitudes with the resulting generation

https://doi.org/10.1017/S0022377822000162 Published online by Cambridge University Press

of longitudinal fields. Dissipative as well as higher-dimensionality effects are therefore under current investigation.

Also, as commented on earlier in the present work, reduction of the group velocity of waves can alternatively be accomplished in a plasma medium. In that case, pump depletion due to snowplough effects adds itself as a factor to be considered in the description of the acceleration process. We note, however, that the passing regime up to the transition point to the accelerating regime may still be described by our proposed corrections.

In the case of tightly guided or focused laser beams with inhomogeneous transversal profiles, some of the accelerating particles not sufficiently aligned with the laser axis will experience transverse forces and be expelled from the central region. For particles aligned with the axis, our theory applies, and for off-axis particles the corresponding dynamics will be hopefully described by an extension of the ponderomotive Hamiltonian described here, an early form of which is under construction.

Acknowledgements

Editor Luís O. Silva thanks the referees for their advice in evaluating this article.

Funding

We acknowledge support from CNPq, Brasil. S.M. thanks the financial support from Grant No. ANR-11-IDEX-0004-02 Plas@Par.

Declaration of interests

The author reports no conflict of interest.

Appendix A

As mentioned, the effective Hamiltonian (3.12) depending only on slow variables can be derived from an appropriate canonical transformation. To perform the transformation, a generating function of the form $F(x, \bar{p}, t) = x\bar{p} + f(x, \bar{p}, t)$ is used, where f comprises a θ dependence such that $\bar{f} = 0$.

The relevant variables transform as

$$p = \bar{p} + \partial f/\partial x, \tag{A1}$$

$$\bar{x} = x + \partial f/\partial \bar{p}, \tag{A2}$$

and

$$\bar{H}_{\text{lin}} = H_{\text{lin}} + \partial f/\partial t. \tag{A3}$$

As in Almansa *et al.* (2019), we demand that the low-frequency canonical Hamiltonian has the form seen in (2.5), but with an added correction term to give an account of the average effects coming from the high-frequency fluctuations

$$\bar{H}_{\text{lin}} = \sqrt{1 + \bar{p}^2 + A_0^2 \exp\left(-\frac{2(x - v_g t)^2}{\sigma^2}\right)} + h(x, \bar{p}). \tag{A4}$$

Note that we express $\bar{H}_{\text{lin}}$ in terms of the independent variables $x, \bar{p}$ of the generating function, deferring the transformation $x \to \bar{x}$ to our last step.

https://doi.org/10.1017/S0022377822000162 Published online by Cambridge University Press

Function $h(x,\bar{p})$ shall play an important role when $v_\phi > 1$, and can be calculated combining (A1), (A3) and (A4) to obtain

$$\sqrt{1+\left(\bar{p}+\frac{\partial f}{\partial x}\right)^2 + A_0^2 \exp\left(-\frac{2(x-v_g t)^2}{\sigma^2}\right)(1-\cos 2\theta)} + \frac{\partial f}{\partial t} = \sqrt{1+\bar{p}^2 + A_0^2 \exp\left(-\frac{2(x-v_g t)^2}{\sigma^2}\right)} + h(x,\bar{p}), \tag{A5}$$

with $\theta = x - v_\phi t$. By transposing the term $\partial f/\partial t$ to the right-hand side of (A5) and squaring both sides, one gets

$$2\bar{H}_{\rm lin}\frac{\partial f}{\partial t} + 2\bar{p}\frac{\partial f}{\partial x} = \left(\frac{\partial f}{\partial t}\right)^2 - \left(\frac{\partial f}{\partial x}\right)^2 + A_0^2 \exp\left(-\frac{2(x-v_g t)^2}{\sigma^2}\right)\cos 2\theta + h(x,\bar{p}). \tag{A6}$$

Equation (A6) is a nonlinear equation for the high-frequency variable f which requires that

$$h(x,\bar{p}) = -\left\langle \left(\frac{\partial f}{\partial t}\right)^2 - \left(\frac{\partial f}{\partial x}\right)^2 \right\rangle_\theta, \tag{A7}$$

to prevent the generation of secular terms in f.

Function h can be calculated if one uses the lowest-order approximation for f, neglecting h and the quadratic terms in (A6) One has

$$2\Gamma\frac{\partial f}{\partial t} + 2\bar{p}\frac{\partial f}{\partial x} = A_0^2 \exp((-2(x-v_g t)^2/\sigma^2))\cos 2\theta. \tag{A8}$$

In (A8) we have used $2\bar{H}_{lin}\partial f/\partial t \approx 2\bar{\Gamma}\partial f/\partial t$, with $\bar{H}_{\rm lin}(h=0) \equiv \Gamma$. Recalling that $f = f(\theta)$, it follows that $\partial f/\partial t = -v_\phi \partial f/\partial x$, and that (A8) can be rewritten as

$$\frac{\partial f}{\partial t} = \frac{A_0^2 \exp\left(\frac{-2(x-v_g t)^2}{\sigma^2}\right)}{2\left(\Gamma - \bar{p}/v_\phi\right)}\cos 2\theta. \tag{A9}$$

From (A9) and (A7) one finally arrives at

$$h(\bar{x},\bar{p}) = -\frac{1}{8}\left(1-\frac{1}{v_\phi^2}\right)\frac{A_0^4 \exp\left(\frac{-4(\bar{x}-v_g t)^2}{\sigma^2}\right)}{\left(\Gamma - \bar{p}/v_\phi\right)^2}, \tag{A10}$$

where x can now be replaced with $\bar{x}$ since it appears only in the slowly modulated amplitude. Therefore, (A10) represents the correction term to be considered in the ponderomotive Hamiltonian when considering a laser pulse with linear polarization. As anticipated, inserting (A10) in (A4) results in the same Hamiltonian shown in (3.12).

REFERENCES

ALMANSA, I., RUSSMAN, F.B., MARINI, S., PETER, E., DE OLIVEIRA, G.I., CAIRNS, R.A. & RIZZATO, F.B. 2019 Ponderomotive and resonant effects in the acceleration of particles by electromagnetic modes. *Phys. Plasmas* **26** (3), 033105.

https://doi.org/10.1017/S0022377822000162 Published online by Cambridge University Press

Burton, D.A., Cairns, R.A., Ersfeld, B., Noble, A., Yoffe, S. & Jaroszynski, D.A. 2017 Observations on the ponderomotive force. In *Relativistic Plasma Waves and Particle Beams as Coherent and Incoherent Radiation Sources II* (ed. D.A. Jaroszynski). International Society for Optics and Photonics. https://spie.org/Publications/Proceedings/Paper/10.1117/12.2270542?SSO=1

Di Piazza, A. 2008 Exact solution of the Landau–Lifshitz equation in a plane wave. *Lett. Math. Phys*. **83**, 305.

Elmore, W.C. & Heald, M.A. 1985 *Physics of Waves*. Dover.

Esarey, E., Sprangle, P., Pilloff, M. & Krall, J. 1995 Theory and group velocity of ultrashort, tightly focused laser pulses. *J. Opt. Soc. Am.* B **12** (9), 1695.

Fedorov, V.Y. & Tzortzakis, S. 2020 Powerful terahertz waves from long-wavelength infrared laser filaments. *Light: Sci. Applics*. **9**, 196.

Goldstein, H. 1980 *Classical Mechanics*. Addison-Wesley.

Harvey, C., Heinzl, T. & Marklund, M. 2011 Symmetry breaking from radiation reaction in ultra-intense laser fields. *Phys. Rev.* D **84**, 116005.

Landau, L. & Lifschitz, E. 1965 *Théorie du champ*. Mir.

Lemos, N., Cardoso, L., Geada, J., Figueira, G., Albert, F. & Dias, J.M. 2018 Guiding of laser pulses in plasma waveguides created by linearly-polarized femtosecond laser pulses. *Sci. Rep*. **8**, 3165.

Liu, C.S. & Tripathi, V.K. 2005 Ponderomotive effect on electron acceleration by plasma wave and betatron resonance in short pulse laser. *Phys. Plasmas* **12**, 043103.

Macchi, A. 1992 *A Superintense Laser-Plasma Interaction Theory Primer*. Springer.

Mendonça, J.T. 2001 *Theory of Photon Acceleration*. Series in Plasma Physics, vol. 218. IOP.

Mulser, P. & Bauer, D. 2010 *High Power Laser-Matter Interaction*. Springer.

Papadopoulos, D.N., Zou, J.P., Le Blanc, C., Chériaux, G., Georges, P., Druon, F., Mennerat, G., Ramirez, P., Martin, L., Fréneaux, A., *et al.* 2016 The apollon 10 pw laser: experimental and theoretical investigation of the temporal characteristics. *High Power Laser Sci. Engng* **4**, e34.

Peng, H., Riconda, C., Grech, M, Zhou, C.-T. & Weber, S. 2020 Dynamical aspects of plasma gratings driven by a static ponderomotive potential. *Plasma Phys. Control. Fusion* **62** (11), 115015.

Ralph, J.E., Marsh, K.A., Pak, A.E., Lu, W., Clayton, C.E., Fang, F., Mori, W.B. & Joshi, C. 2009 Self-guiding of ultrashort, relativistically intense laser pulses through underdense plasmas in the blowout regime. *Phys. Rev. Lett*. **102**, 175003.

Robinson, A.P.L. 2021 A critical analysis of the 'ponderomotive snowplow' concept in direct laser acceleration of electrons. *Plasma Phys. Control. Fusion* **93** (6), 064003.

Ruiz, D.E. & Dodin, I.Y. 2017 Ponderomotive dynamics of waves in quasiperiodically modulated media. *Phys. Rev.* A **95**, 032114.

Russman, F., Almansa, I., Peter, E., Marini, S. & Rizzato, F.B. 2020 Non-resonant acceleration of charged particles driven by the associated effects of the radiation reaction. *J. Plasma Phys*. **86** (5), 905860513.

Sazegari, V., Mirzaie, M. & Shokri, B. 2006 Ponderomotive acceleration of electrons in the interaction of arbitrarily polarized laser pulse with a tenuous plasma. *Phys. Plasmas* **13**, 033102.

Shukla, P.K., Rao, N.N., Yu, M.Y.L. & Tsintsadze, N.L. 1986 Relativistic nonlinear effects in plasmas. *Phys. Rep*. **138**, 1–149.

Smorenburg, P.W., Kamp, L.P.J., Geloni, G.A. & Luiten, O.J. 2010 Coherently enhanced radiation reaction effects in laser-vacuum acceleration of electron bunches. *Laser Part. Beams* **28** (4), 553.

Startsev, E.A. & McKinstrie, C.J. 1997 Multiple scale derivation of the relativistic ponderomotive force. *Phys. Rev.* E **55**, 7527.

Steinhauer, L.C. & Kimura, W.D. 2003 Slow waves in microchannel metal waveguides and application to particle acceleration. *Phys. Rev. ST Accel. Beams* **6**, 061302.

Terzani, D., Benedetti, C., Schroeder, C.B. & Esarey, E. 2021 Accuracy of the time-averaged ponderomotive approximation for laser-plasma accelerator modeling. *Phys. Plasmas* **28** (6), 063105.

Vranic, M., Martins, J.L., Vieira, J., Fonseca, R.A. & Silva, L.O. 2014 All-optical radiation reaction at 10^{21} w cm^{-2}. *Phys. Rev. Lett*. **113**, 134801.